OPEN ACCESS
IOP Publishing
Journal of Physics G: Nuclear and Particle Physics
J. Phys. G: Nucl. Part. Phys. **47** (2020) 085102 (11pp)
https://doi.org/10.1088/1361-6471/ab920b

Cross-section, vector and tensor analyzing powers of the ^{6}Li $+^{12}$C elastic scattering at 30 and 50 MeV: a non-monotonic potential description

A Nilima[1,2,5], S Hossain[3], M M B Azad[4], M M Billah[4], A S B Tariq[4] and A K Basak[4]

[1] School of Physics and Astronomy, University of Edinburgh, United Kingdom
[2] Department of Physics, University of Dhaka, Dhaka, Bangladesh
[3] Department of Physics, Shahjalal University of Science & Technology, Sylhet, Bangladesh
[4] Department of Physics, University of Rajshahi, Rajshahi, Bangladesh

E-mail: athoynilima@gmail.com

Received 13 January 2020, revised 24 April 2020
Accepted for publication 11 May 2020
Published 23 June 2020

Abstract

This work reports, for the first time, the analysis of tensor analyzing powers (T_{20}, T_{21}, T_{22}) along with the differential cross-section (CS) and the vector analyzing power iT_{11} for the ^{6}Li $+^{12}$C elastic scattering at 30 and 50 MeV within the framework of an optical model (OM) using microscopic shallow non-monotonic (NM) potentials. The NM potential is generated from the energy density functional formalism (EDF) (Brueckner *et al* (1968) *Phys. Rev.* **168** 1184) using a realistic two-nucleon interaction incorporating the Pauli exclusion principle. The shallow NM potential can describe the experimental angular distributions of CS and analyzing powers of the elastic scattering data. The OM analysis of the data at 30 and 50 MeV does not indicate their sensitivity on the nuclear matter incompressibility K.

Keywords: non-monotonic potential, ^{6}Li + ^{12}C elastic scattering, nuclear incompressibility, TAP, VAP

(Some figures may appear in colour only in the online journal)

[5]Author to whom any correspondence should be addressed.

1. Introduction

The elastic scattering of ^{6}Li on ^{12}C has been of considerable interest over the past few decades, not only because they exhibit interesting transitional features [1] between the light (mass number, $A \leqslant 4$) and heavy ($A \leqslant 12$) ions, but also for the strong refractive [2] nature of its angular distribution [3]. In combination with a weak absorption, the refractive effect gives rise to nuclear rainbow, i.e. large angle Airy oscillations followed by an exponential fall-off. Generally, they are not expected to manifest in scattering of loosely bound nuclei (e.g. ^{6}Li) because of the suppression caused by projectile breakup effect [4]. The refractive ^{6}Li $+^{12}$ C scattering is clearly an exception, and it was attributed [5] to the distinguishing cluster ($\alpha + d$) structure in ^{6}Li. The knowledge of projectile-target potential between ^{6}Li and ^{12}C thus holds the key to shed some light on the present understanding of nuclear structure and interactions in the nuclear realm. An understanding of the interaction between lithium isotopes, the heaviest formed in primordial nucleosynthesis, is likely to be important for understanding of stellar synthesis of heavier species.

As noted by Pakou *et al* [6, 7], the widely used microscopic potentials of ^{6,7}Li-nucleus from double folding (DF) need an energy-dependent renormalization of $N_{\mathrm{R}} = 0.5$–0.7 to reproduce the experimental cross section (CS) data. Sakuragi and his group [4, 8, 9] elegantly demonstrated that the large N_{R} can be done away with the use of the continuum-discretized coupled channels (CDCC) method. A CDCC calculation generates a repulsive dynamic polarization potential (DPP) to take care of N_{R}. Moreover, as shown by [10, 11], the large vector analyzing powers (VAP) of ^{6,7}Li-nucleus elastic scattering can be generated by the DPP originated in coupled channel (CC) and CDCC calculations.

Microscopic potentials, derived from the energy density functional (EDF) theory [12] incorporates the Pauli effect of anti-symmetrization, and are non-monotonic (NM) and shallow [13]. They account well for α elastic scattering [[13], and references therein] and α induced non-elastic processes [14–18] including the band-mixing of rotational states with bandheads $I^{\pi} = \frac{1}{2}^{+}$ and $\frac{3}{2}^{+}$ [19] in ^{29}Si and ^{29}P. The NM potentials are also found successful to reproduce the prominent refractive pattern in the ^{16}O $+^{16}$O elastic scattering [20]. Also the sensitivity of NM potentials on the incompressibility K for cold nuclear matter as elucidated in [20] opens a doorway to deduce the value of K. The repulsive real part in the EDF-derived NM potential can also generate the effects of DPP through simple CC as shown in Basak *et al* [11], to describe satisfactorily VAP in ^{6}Li $+^{28}$Si scattering without needing either renormalization in the NM potential or any static spin–orbit (SO) potential. The NM potentials are also found to reproduce in the simple optical model (OM) by Basak *et al* [21] the magnitudes and opposite signs of VAP of ^{6}Li and ^{7}Li elastic scattering by ^{58}Ni at $E_{\mathrm{lab}} = 20$ MeV and by ^{120}Sn at 44 MeV in addition to the CS data again without requiring a renormalization. The success of the NM potentials has been ascribed mainly to the microscopic consideration of the Pauli principle in the EDF theory. The various successes enjoyed by the NM potentials have stimulated us to undertake the present investigation. Reber *et al* [22] and Kerr *et al* [23] applied successfully a J-dependent absorption in the framework of OM to describe their experimental data of VAP (iT_{11}) and tensor analyzing powers (TAPs), T_{20}, T_{21} and T_{22} at 30 and 50 MeV after introducing the Thomas spin–orbit SO and complex tensor T_{R} of [24–26].

This article reports the performance of NM potentials to describe the refractive ^{6}Li $+^{12}$C elastic scattering data on CS, iT_{11} and TAPs, T_{20}, T_{21} and T_{22} at 30 and 50 MeV in the simple OM potential for the first time.

2. Non-monotonic potentials for ^{6}Li $+^{12}$C system

2.1. EDF formalism

The EDF theory [12] describes the energy of a fermionic system as

$$E = \int \epsilon \left[\rho(\vec{r})\right] \mathrm{d}^3\vec{r}, \tag{1}$$

where $\rho(r)$ is the density distribution (DD) of the system and $\epsilon\left[\rho(\vec{r})\right]$ is the energy density [19]:

$$\epsilon\left[\rho(\vec{r})\right] = B(\rho,\xi)\rho + \left(\frac{\hbar^2}{8M}\right)\eta(\nabla\rho)^2 + \text{Coulomb terms}. \tag{2}$$

For symmetric nuclei like ^{6}Li and ^{12}C, the neutron excess, $\xi = (N-Z)/A = 0$, and the binding energy per nucleon of the system $B(\rho,\xi)$ read as [20]

$$B(\rho,\xi=0) = 0.3\left(\frac{\hbar^2}{M}\right)\left(\frac{3\pi^2}{2}\right)^{2/3}\rho^{2/3} + v(\rho,\xi=0), \tag{3}$$

where M is the nucleon mass, and $v(\rho,\xi)$ is the nucleonic mean field. For infinite symmetric nuclear matter (ISNM) [20, 27],

$$v(\rho,\xi=0) = \lambda_1\rho + \lambda_2\rho^{4/3} + \lambda_3\rho^{5/3}. \tag{4}$$

To apply to finite nuclei, two correction terms are incorporated in equation (2): the inhomogeneity correction[6] term with a free parameter η, and the Coulomb (last two) terms.

The density-dependent mass formula embodied in the EDF (equation (2)) provides information on the nuclear equation of state (EOS) (i.e. the energy per nucleon, E/A, as a function of density) and on the compressibility of nuclear matter at various densities including the saturation density ρ_0. The curvature of $E/A(\rho)$ of nuclear matter around the saturation point $\rho = \rho_0$ is termed as the nuclear incompressibility:

$$K = 9\rho^2\left[\frac{\partial^2}{\partial\rho^2}\left(\frac{E}{A}\right)\right]_{\rho=\rho_0}. \tag{5}$$

2.2. EDF calculations for the ^{6}Li + ^{12}C system

A detailed discussion on the derivation of NM potentials from the EDF theory and the sensitivity of the EDF potentials on K can be found in [13, 20]. We mention here only the salient points on their derivation from EDF.

In the EDF calculations, the density distribution (DD) of the composite system is calculated assuming a sudden approximation, i.e. as a simple sum of the density distributions (DDs) of the projectile and the target nucleus. The parameters of the original DD functions of ^{6}Li and ^{12}C, respectively, from [28, 29], are transformed to the two-parameter Fermi (2pF) function,

$$\rho(r) = \rho_0[1 + \exp\{(r-c)/z\}]^{-1}, \tag{6}$$

[6] It incorporates the part of nuclear interaction that is not included in the mean field.

Table 1. The parameters of the equivalent 2pF DD function for ^{6}Li and ^{12}C nuclei with the calculated (Calc.) and experimental (Expt.) binding energies.

	2 pF DD parameters			Binding energy	
Nucleus	c (fm)	z (fm)	ρ_0 (fm^{-3})	Calc. (MeV)	Expt. (MeV)
^{6}Li	1.333	0.577	0.2118	33.1	32.0
^{12}C	2.294	0.434	0.1752	91.9	92.2

Table 2. Mean-field parameters (λ), the volume integral per nucleon pair ($J_{\rm R}/72$) for the EDF-derived potentials and the inhomogeneity parameter η for two different K values.

K(MeV)	λ_1	λ_2	λ_3	η	$J_{\rm R}/72$ (MeV fm^3)
188	−741.28	+1179.55	−467.54	8.0	−145.25
219	−756.50	+1195.53	−451.07	8.95	−143.75

for use in the EDF calculations. The equivalent parameters of the 2pF function are taken from [21] and given in table 1.

The potential $V(R)$ (sum of nuclear and Coulomb parts) between the ^{6}Li projectile and the ^{12}C target at a separation distance of R is given [13, 20] by

$$V(R) = E[\rho_c(\vec{r}, R)] - E[\rho_1(\vec{r}, R)] - E[\rho_2(\vec{r}, R)]. \tag{7}$$

Here $\rho_1(\vec{r})$ and $\rho_2(\vec{r})$ are, respectively, the DD functions of ^{6}Li and ^{12}C with their parameters in table 1. $\rho_c(\vec{r}) = \rho_1(\vec{r}) + \rho_2(\vec{r})$ refers to DD of the composite nucleus in the sudden approximation. Es are the total energies of the individual nuclei including the mean-field $v(\rho, \xi = 0)$ in the nuclear matter with K in equation (5).

EDF potentials for two different K-values, $K = 188$ MeV and $K = 219$ MeV are generated. The mean-field parameters for homogeneous ISNM (table 2) are taken from [20, 30] for $K = 188$ MeV and those for $K = 219$ MeV are computed following the procedure of [20].

Finally, the ^{6}Li + ^{12}C potentials are derived by employing the DD parameters from table 1 and the mean-field parameters from table 2 in the EDF theory. In achieving these, the inhomogeneity parameter for $K = 188$ MeV is $\eta = 8$ as in [13, 14, 21, 22] while that for $K = 219$ MeV is adjusted to $\eta = 8.95$ (table 2) to reproduce the experimental binding energies of ^{6}Li and ^{12}C as noted in table 1.

The reliability of the EDF-generated NM potential can be assured from the favourable closeness of the experimental binding energies of the colliding nuclei (see table 1) with the EDF-calculated values from the chosen DD parameters in conjunction with the mean-field parameters λ_1, λ_2, λ_3, and the inhomogeneity η parameters in table 2. The volume integral $J_{\rm R}/72$ values in table 2 reflect their dependence on K.

2.3. Potential parametrisation

The EDF-generated potential points of $V(R)$ are parametrized with the analytic expression:

$$V_{\rm N}(R) = -V_0\left[1 + \exp\left(\frac{R - R_0}{a_0}\right)\right]^{-1} + V_1 \exp\left[-\left(\frac{R - D_1}{R_1}\right)^2\right]. \tag{8}$$

Table 3. Nuclear real parameters for the ^{6}Li $+^{12}$ C central potential with $J_R/72$-values and χ^2 per degree of freedom (d.o.f.) for the fits. The Coulomb radius is $R_C = 3.612$ fm. The parameters of the EDF-188 and EDF-219 sets correspond the EDF-derived potentials for $K = 188$ and $K = 219$ MeV, respectively. Set-1 and set-2 refer to the sets of parameters, all adjusted empirically for a best possible fit to the 30 and 50 MeV experimental data, respectively. E_{lab}, V_0 and V_1 are in MeV; R_0, R_1, a_0 and D_1, in fm; and $J_R/72$, in MeV fm^3.

Set	E_{lab}	V_0	R_0	a_0	V_1	R_1	D_1	$J_R/72$	χ^2/d.o.f.
EDF-188	30/50	37.3	4.00	0.736	33.8	2.43	0.133	−145.25	388.9
EDF-219	30/50	41.0	4.00	0.734	46.7	2.49	0.118	−143.75	342.3
Set-1	30	28.0	4.602	0.54	75.0	0.35	2.175	−141.2	18.0
Set-2	50	32.0	4.006	0.82	150.0	0.47	1.076	−141.0	15.3

In the parameterization procedure, the EDF-derived potential points are found best described by $R_0 = 4.0$ fm with other parameters obtained by an analytic fit to potential points. The potential parameters, thus derived, are listed in table 3. The parameterized $V_N(R)$ in equation (8) serves as the real part of the central potential in our complex optical potential (OP) which is given by

$$U(R) = V_C(R) + V_N(R) + iW(R) + U_{SO}(R) + U_{TR}(R), \tag{9}$$

where $V_C(R)$, $V_N(R)$ and $W(R)$ denote, respectively, the Coulomb, nuclear real and nuclear imaginary potentials. $V_C(R)$ is assumed to be that due to a uniformly charged sphere of radius R_C.

The central imaginary part $W(R)$, assumed in the analysis, comprises a Gaussian-shaped volume term and a surface term with a shifted Gaussian shape:

$$W(R) = -W_0 \ \exp\left[-\left(\frac{R}{R_W}\right)^2\right] - W_S \ \exp\left[-\left(\frac{R-D_S}{R_S}\right)^2\right]. \tag{10}$$

An effective spin–orbit (SO) potential with a standard Woods–Saxon (WS) form is considered:

$$U_{SO}(R) = 2\frac{V_{SO}}{R}\ \frac{d}{dR}[1 + \exp((R - R_{SO})/a_{SO})]^{-1}\vec{l}\cdot\vec{I}, \tag{11}$$

where $\vec{l}$ and $\vec{I}$ are, respectively, the partial wave angular momentum and spin of ^{6}Li.

The tensor part of the ^{6}Li potential is complex, and taken from Reber *et al* [22]:

$$U_{TR}(R) = -\frac{8}{6\sqrt{3}}\left[V_T a_{RT}^2 \frac{d^2}{dR^2} f_R(R) + iW_T a_{iT}^2 \frac{d^2}{dR^2} f_I(R)\right]\left[(\vec{I}\cdot\hat{R})^2 - 2/3\right], \tag{12}$$

where $\hat{R}$ refers to the unit vector along $\vec{R}$. The form factors in equation (12) are defined as

$$f_x(R) = [1 + \exp\{(R - R_x)/a_x\}]^{-1}. \tag{13}$$

Table 4. Same as in table 3 for the imaginary potential parameters with the corresponding volume integral per nucleon-pair $J_I/72$ and the parameters of SO part of the OM potential. $J_I/72$ is in MeV fm^3 and the depth and geometry parameters are, respectively, in MeV and fm. E_{lab} is in MeV.

Set	E_{lab}	W_S	D_S	R_S	W_0	R_W	V_{SO}	R_{SO}	a_{SO}	$J_I/72$
EDF-188	30	25.0	3.365	0.22	13.0	4.0	0.15	5.495	0.17	−83.7
	50	5.0	5.723	0.12	17.5	4.0	0.16	5.678	0.10	−92.8
EDF-219	30	25.0	3.365	0.22	13.0	4.0	0.15	5.495	0.17	−83.7
	50	5.0	5.723	0.12	17.5	4.0	0.16	5.678	0.10	−92.8
Set-1	30	21.0	4.396	0.10	14.0	3.9	0.4	5.266	0.55	−76.1
Set-2	50	5.8	5.952	0.10	19.0	3.9	0.12	5.941	0.10	−93.5

3. Analysis and results

The experimental CS, iT_{11}, T_{20}, T_{21} and T_{22} data for the ^{6}Li + ^{12}C elastic scattering are taken from [22, 23, 31]. The CS data are normalized to the Rutherford cross-sections, and a systematic error of 15% is assumed for the CS points without any experimental error-bar. The OM analyses are carried out using the code SFRESCO that incorporates the coupled-channels code FRESCO2.5 [32] and is coupled with the χ^2-minimization code MINUIT [33]. The fitting parameters are obtained by minimizing χ^2, normalized per degree of freedom $(N - F)$ where N is the number of data points for a given incident energy and F is the number of adjusted parameters. The χ^2 per degree of freedom is referred as simply χ^2 hereinafter in the text. The Coulomb radius is set to $R_C = 3.612$ fm.

3.1. Fits with EDF-generated nuclear real part

At the onset, we choose the EDF-derived central potential $V_N(R)$ for $K = 188$ MeV given in table 3. Firstly, the parameters of the real central part $V_N(R)$ are kept unchanged and the parameters for the imaginary $W(R)$ and those of SO $U_{SO}(R)$ are optimized through a sequence of grid and global searches to minimize χ^2 in fitting the experimental σ/σ_R and iT_{11} data. Next, the parameters of tensor part $U_{TR}(R)$ are searched upon to minimize χ^2 in fitting the iT_{11}, T_{20}, T_{21} and T_{22} data. In the third step, all parameters of $W(R)$, $U_{SO}(R)$ and $U_{TR}(R)$ are readjusted to improve description of the σ/σ_R, iT_{11}, T_{20}, T_{21} and T_{22} data. The final fits have been done *visually* after taking guidance from the χ^2 fits, since it is more important to reproduce the features in the angular distributions of the experimental data than naively minimizing the χ^2 only [34].

For the EDF-219 potential set with $K = 219$ MeV, which is close to the derived value of $K = 222 \pm 5$ MeV for the infinite cold nuclear matter by Hossain *et al* [20], the third and the final steps have been accomplished in optimizing all the parameters excepting those of the EDF-derived $V_N(R)$ using the experimental data of σ/σ_R, iT_{11}, T_{20}, T_{21} and T_{22}. The χ^2 for the best fits and the associated volume integrals $J_R/72$ and $J_I/72$, respectively, for the real and imaginary parts of OP are also listed in tables 3, 4 and 5.

The predicted values from the OM calculations are compared with the experimental data in figures 1 and 2 for 30 and 50 MeV projectile energies. Our OM results for 5 observables σ/σ_R, iT_{11}, T_{20}, T_{21} and T_{22} calculated using the EDF potentials for $K = 188$ and 219 MeV are found almost similar and describe the experimental data reasonably well excepting the case of T_{20} at 50 MeV, where the dip at the scattering angle of 55° and the bump at 80° could

Table 5. Same as in table 4 for the tensor part of the OM potential and χ^2/d.o.f. for the fits.

Set	$E_{\rm lab}$	$V_{\rm T}$	$R_{\rm RT}$	$a_{\rm RT}$	$W_{\rm T}$	$R_{\rm IT}$	$A_{\rm IT}$	χ^2/d.o.f.
EDF-188	30	+0.234	4.304	0.45	—	—	—	388.9
	50	−0.140	4.922	0.55	—	—	—	50.0
EDF-219	30	+0.234	4.304	0.45	—	—	—	342.3
	50	−0.140	4.922	0.55	—	—	—	44.0
Set-1	30	+0.173	4.235	0.30	−0.488	3.892	0.65	18.0
Set-2	50	−0, 135	5.151	0.50	—	—	—	10.1

not be reproduced. For the 30 MeV scattering, a small peak at $\theta_{\rm CM} = 35^\circ$ in the experimental data of T_{20} is not reproduced by OM calculations.

Although the χ^2 for the fits with the EDF-219 potential set is slightly lowered over that for the EDF-188 set, as can be noted in table 3, no significant improvement in the data description can be sighted in the visual inspection of figures 1 and 2. This can be explained by the fact that at both of 30 and 50 MeV incident energies, ^{6}Li does not carry adequate energies to reach the nuclear interior with $R \leqslant 3$ fm where the EDF-188 and EDF-219 potentials show some difference (see figures 1 and 2).

3.2. *Fits with empirically adjusted nuclear real part*

All experimental data at the $E_{\rm lab} = 30$ and 50 MeV energies are re-analysed after freeing the EDF-generated potential-parameters for adjustment in order to obtain better quality fits to the experimental data. In the process, the parameters of the imaginary, SO and tensor parameters are further tuned. This approach results in much better descriptions of data with much reduction in the respective χ^2 values and the final parameters are presented in tables 3–5 as set-1 for 30 MeV and set-2 for 50 MeV.

It should be noted here that the EDF-theory does not have *an energy-dependent factor* built in it, and the EDF-generated potential is valid at low energies strictly at the zero excitation energy of the composite nucleus, as observed in [20]. At higher incident energies, as our previous work on $\alpha + ^{90}$Zr [13] suggests that the position D_1 of the repulsive core moves towards the surface region with increasing incident energy due to the changing configuration of the nucleons in the composite nucleus formed during the interaction of the projectile and the target, leading to the different Pauli effects.

However, the predictions with the empirically adjusted nuclear part of the central potential fail to improve description of the T_{20} data beyond $\Theta_{\rm CM} = 40^\circ$. The predicted $\sigma/\sigma_{\rm R}$, iT_{11}, T_{20}, T_{21} and T_{22} are compared with the experimental data in figure 2. In particular, the empirical set-1 potential for 30 MeV predicts the opposite signs of T_{20} analyzing powers near the dip in experimental distribution around the scattering angle $\Theta_{\rm CM} = 55^\circ$, reproduced well by the EDF-188 potential in figure 1.

Improvement in the description of the experimental data using the empirical potentials, particularly forging it in the cross section data, leads to radial distributions of the set-1 and set-2 potentials very different from the EDF-derived, EDF-188 and EDF-219 potential sets in figures 1 and 2. The increased repulsive behaviour of the empirical sets inside the nuclear surface is likely to be linked to the dispersive effect at the onset of non-elastic channels leading to a repulsive surface potential in the real part [35, 36].

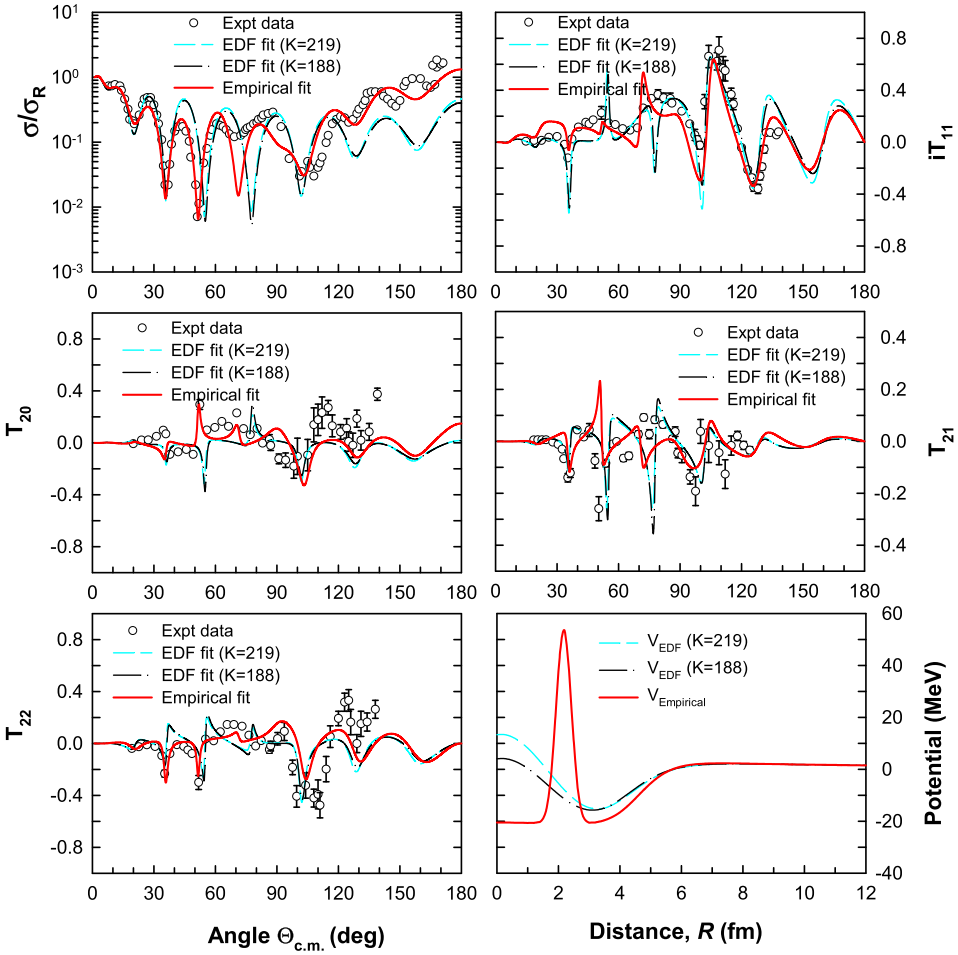

Figure 1. Predicted $\sigma/\sigma_{\rm R}$, iT_{11}, T_{20} and T_{22} for the ^{6}Li + ^{12}C elastic scattering at 30 MeV by the OM potentials with the real central nuclear parts (a) EDF-derived for $K = 188$ MeV (dash-dot lines), (b) EDF-derived for $K = 219$ MeV (dash-dash lines) and (c) from empirically adjusted (solid lines) are compared with the experimental data. The central real parts of the nuclear potentials are also displayed to show their NM feature.

4. Discussion and conclusions

The study examines for the first time the NM potential, embodying a repulsive core, on the tensor analyzing powers in the framework of simple OM potential. The $T_{\rm R}$ tensor potential, originally proposed Satchler [24] and tried on the ^{6}Li + ^{12}C scattering by Reber *et al* [22, 37] and Kerr *et al* [23, 38], in conjunction with the NM central real, effective SO and imaginary parts of the interaction potential $U(R)$ in equation (9), are able to reproduce features in the angular distributions of CS and analyzing power data. In particular, iT_{11}, T_{21}, T_{22} data are well accounted for in OM using normal J-independent imaginary potential. In the overall picture, our predictions seem to have reproduced the experimental data somewhat better than the calculations reported in [22, 23] involving the J-dependent absorption and are

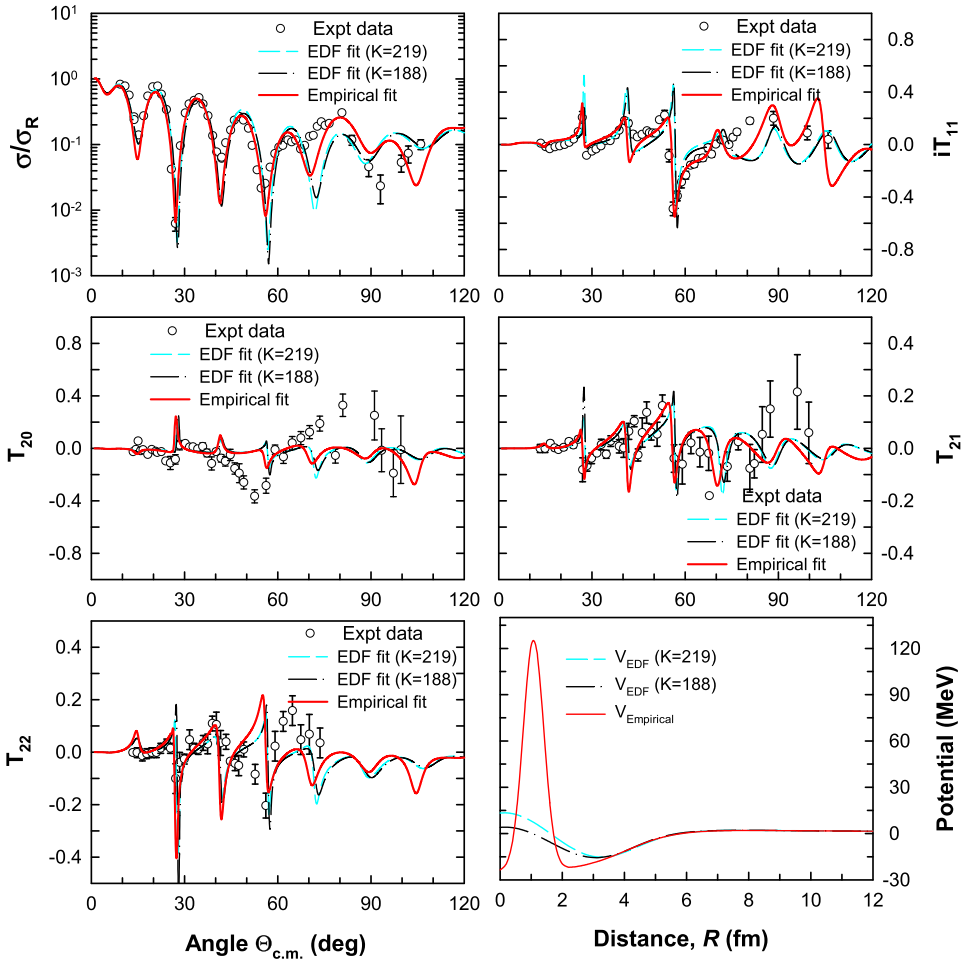

Figure 2. Same as in figure 1 for ^{6}Li $+^{12}$ C elastic scattering at 50 MeV.

found to be no less inferior to the findings from the coupled-channels (CC) calculations in [37, 38]. However, our calculations provide a poor show in the description of the experimental T_{20} data at both energies considered herein. Our study confirms the observation of [22, 23] that T_{21} is most sensitive to the central and tensor U_{TR} interactions. Other analyzing powers are sensitive to central, SO and tensor terms.

Satisfactory performance of our NM potentials in describing the CS and analyzing power data suggests two important points. Firstly that the action of the repulsive core not only plays the role of the equivalent dynamic polarization potential partially, which in conjunction with a static SO potential, can remove the renormalization problem with the DF potentials [4, 8, 9] and solve the enigma of the opposite signs of the VAPs in the ^{6}Li and ^{7}Li elastic scattering by the same target nucleus [10]. Use of the Pauli-based repulsive core in the EDF-generated NM potentials has shown to produce the same effects [11, 21] in OM. As the repulsive core in our framework is understood to emerge from the Pauli blocking embedded in our EDF formalism, our conjecture has been that Pauli blocking reproduces DPP, at least partially, even in OM. However, the seemingly large empirical adjustment of the real

repulsion reported in the present work needs to be studied further. We suspect that the large difference between the EDF sets and the empirical NM potentials may lie in forging fits to the experimental CS data (figures 1 and 2), which may involve contributions from non-direct processes. It is expected that future work will make it clear how much of the DPP and breakup effects can be explained solely through an EDF-based approach. Secondly, the repulsive core associated with the NM potential in equation (8), although J-independent, does the job of J-dependent absorption [22, 23] as it simulates an l-dependent barrier potential which attenuates more of the lower partial waves than the higher ones. The latter accrues the satisfactory descriptions of data in the simple OM by EDF-originated NM potentials in the present work.

Our work does not show significant K-dependence on the predicted $\sigma/\sigma_{\rm R}$, iT_{11}, T_{20}, T_{21} and T_{22} at both projectile energies of 30 and 50 MeV. This is evidenced in the small difference between the χ^2 values fittings the experimental data using the EDF-188 and EDF-219 potentials at each of incident energies (see table 5). This is not surprising as at lower energies surface effect dominates the elastic scattering while K-dependence of the EDF-derived potential occurs in the nuclear interior with $R \leqslant 3$ fm (see figures 1 and 2). The scattering from the nuclear interior contributes to the refractive scattering as discussed in [3, 13, 20, 39]. Michel and Ohkubo in [39] suggest that the broad dip at $\theta_{\rm CM} \sim 105^\circ$ in the CS distribution of $E_{\rm lab} = 30$ MeV is due to the second Airy minimum (A2) arising from the refractive scattering. The potential effect at the same radial position of nuclear interior as producing the A2 minimum does not have adequately strong K-dependence to induce a conspicuous K-sensitive effect on the CS and analyzing powers. One needs to study the elastic scattering at higher energies where first Airy minimum A1 following by nuclear rainbow scattering with exponent-type falloff in cross sections [20, 40, 41] is visible in the CS angular distribution.

It remains to investigate why T_{20} beyond the scattering angle $\theta_{\rm CM} \sim 40^\circ$ at $E_{\rm lab} = 50$ MeV could not be reproduced even with the empirical adjustment of the EDF-generated NM potentials for the real part of the central potential. It may be related to a correlated effects from the central, SO, tensor and also additional DPP arising from coupling to the resonant breakup states of ^{6}Li and inelastic states of ^{12}C, not considered in the present work.

Acknowledgments

We are thankful to Krzysztof Rusek for useful comments and to Ian J Thompson for his code SFRESCO and assistance with using it.

ORCID iDs

A Nilima https://orcid.org/0000-0001-9606-2676
M M Billah https://orcid.org/0000-0001-6987-0977

References

[1] DeVries R M, Goldberg D A, Watson J W, Zisman M S and Cramer J G 1977 *Phys. Rev. Lett.* **39** 450–3
[2] Brandan M and Satchler G 1997 *Phys. Rep.* **285** 143–243
[3] Khoa D T, Satchler G R and von Oertzen W 1995 *Phys. Rev.* C **51** 2069–84
[4] Sakuragi Y 1987 *Phys. Rev.* C **35** 2161–74

[5] Khoa D T, von Oertzen W, Bohlen H G and Ohkubo S 2007 *J. Phys. G: Nucl. Part. Phys.* **34** R111–64
[6] Pakou A *et al* 2003 *Phys. Lett.* B **556** 21–6
[7] Pakou A 2008 *Phys. Rev.* C **78** 067601
[8] Hirabayashi Y and Sakuragi Y 1992 *Nucl. Phys.* A **536** 375–96
[9] Sakuragi Y, Yahiro M and Kamimura M 1986 *Prog. Theor. Phys. Suppl.* **89** 136
[10] Hirabayashi Y, Sakuragi Y and Tanifuji M 1993 *Phys. Lett.* B **318** 32–8
[11] Basak A K, Roy P K, Hossain S, Abdullah M N A, Tariq A S B, Uddin M A, Reichstein I and Malik F B 2010 *Phys. Lett.* B **692** 47–50
[12] Brueckner K A, Coon S A and Dabrowski J 1968 *Phys. Rev.* **168** 1184–8
[13] Hossain S *et al* 2013 *J. Phys. G: Nucl. Part. Phys.* **40** 105109
[14] Basak A, Abdullah M, Tariq A, Das S, Rahman A, Mondal A, Sen Gupta H and Malik F 2001 *Eur. Phys. J.* A **12** 387–97
[15] Das S K, Tariq A S B, Rahman A F M M, Roy P K, Huda M N, Mondal A S, Basak A K, Sen Gupta H M and Malik F B 1999 *Phys. Rev.* C **60** 044617
[16] Das S K, Tariq A S B, Uddin M A, Mondal A S, Basak A K, Rashid K M, Sen Gupta H M and Malik F B 2000 *Phys. Rev.* C **62** 054605
[17] Das S K, Tariq A S B, Rahman A F M M, Hossain S, Mondal A S, Basak A K, Sen Gupta H M and Malik F B 2001 *Phys. Rev.* C **64** 034605
[18] Das S K, Basak A K, Banu K, Mondal A S, Tariq A S B, Rahman A F M M, Sen Gupta H M and Malik F B 2000 *Phys. Rev.* C **62** 054606
[19] Hossain S, Abdullah M N A, Das S K, Uddin M A, Basak A K, Gupta H M S, Thompson I J and Malik F B 2005 *J. Phys. G: Nucl. Part. Phys.* **31** 309–19
[20] Hossain S *et al* 2015 *Phys. Rev.* C **91** 064613
[21] Basak A K *et al* 2011 *Europhys. Lett.* **94** 62002
[22] Reber E L, Kemper K W, Green P V, Kerr P L, Mendez A J, Myers E G and Schmidt B G 1994 *Phys. Rev.* C **49** R1–4
[23] Kerr P L, Kemper K W, Green P V, Mohajeri K, Myers E G, Robson D and Schmidt B G 1995 *Phys. Rev.* C **52** 1924–33
[24] Satchler G 1960 *Nucl. Phys.* **21** 116–27
[25] Raynal J 1963 *Phys. Lett.* **3** 331–3
[26] Irshad M and Robson B 1974 *Nucl. Phys.* A **218** 504–8
[27] Malik F and Reichstein I 1992 *Clustering Phenomena in Atoms and Nuclei* (Berlin: Springer)
[28] Bray K H, Jain M, Jayaraman K S, Lobianco G, Moss G A, van Oers W T H, Wells D O and Petrovich F 1972 *Nucl. Phys.* A **189** 35–64
[29] Sick I 1974 *Nucl. Phys.* A **218** 509–41
[30] Hooshyar M A, Reichstein I and Malik F B 2005 *Nuclear Fission and Cluster Radioactivity: an Energy-Density Functional Approach* (Berlin: Springer)
[31] Vineyard M F, Cook J, Kemper K W and Stephens M N 1984 *Phys. Rev.* C **30** 916–24
[32] Thompson I J 1988 *Comput. Phys. Rep.* **7** 167–212
[33] James F and Roos M 1975 *Comput. Phys. Commun.* **10** 343–67
[34] Koning A and Delaroche J 2003 *Nucl. Phys.* A **713** 231–310
[35] Nagarajan M A, Mahaux C C and Satchler G R 1985 *Phys. Rev. Lett.* **54** 1136–8
[36] Mahaux C, Ngo H and Satchler G R 1986 *Nucl. Phys.* A **449** 354–94
[37] Reber E L, Kemper K W, Green P V, Kerr P L, Mendez A J, Myers E G, Schmidt B G and Hnizdo V 1994 *Phys. Rev.* C **50** 2917–26
[38] Kerr P L, Kemper K W, Green P V, Mohajeri K, Myers E G, Schmidt B G and Hnizdo V 1996 *Phys. Rev.* C **54** 1267–81
[39] Michel F and Ohkubo S 2005 *Phys. Rev.* C **72** 054601
[40] Goldberg D A and Smith S M 1972 *Phys. Rev. Lett.* **29** 500–3
[41] Khoa D T, von Oertzen W, Bohlen H and Nuoffer F 2000 *Nucl. Phys.* A **672** 387–416